Solid-state NMR, X-ray diffraction and theoretical studies of neutral mononuclear molecular bis(triphenylphosphine)silver(I) mono-carboxylate and nitrate systems

Simon Grabowsky,[a,*] Allan H. White,[b,#] Peter C. Healy,[c] Kim M. Lapere,[d] Seik Weng Ng,[e] Brian W. Skelton,[b] Duncan A. Wild,[b] Graham A. Bowmaker,[f,*] and John V. Hanna[g,*]

[a] University of Bern, Department of Chemistry and Biochemistry, Freiestrasse 3, 3012 Bern, Switzerland

[b] University of Western Australia, School of Molecular Sciences, 35 Stirling Highway, Perth, WA 6009, Australia

[c] Griffith University, School of Environment and Science, 170 Kessels Road, Nathan, 4111 Queensland, Australia

[d] University of New South Wales, School of Chemistry, Sydney, 2052 New South Wales, Australia

[e] University of Malaya, Department of Chemistry, 50603 Kuala Lumpur, Malaysia

[f] University of Auckland, School of Chemical Sciences, Private Bag 92019, Auckland 1142, New Zealand

[g] University of Warwick, Department of Physics, Gibbet Hill Rd., Coventry CV4 7AL, UK

Professor Allan H. White is deceased.

* Corresponding authors e-mail addresses: simon.grabowsky@dcb.unibe.ch, g.bowmaker@auckland.ac.nz, j.v.hanna@warwick.ac.uk

Abstract

Neutral mononuclear molecular silver(I) carboxylate complexes of the form $[(Ph_3P)_2Ag(O_2XY)]$ with O_2XY = O_2CCH_2Ph, O_2CCHPh_2, $O_2CC(CH_3)_3$, $O_2CCH_2C(CH_3)_3$, O_2CCF_3 (compounds **1**-**4** and **5β**) have been investigated in the solid state using single-crystal X-ray structure determinations, 1D ^{31}P CPMAS NMR and 2D ^{31}P-^{31}P CPCOSY NMR measurements, and *ab-initio* computational modeling. The results show that these complexes contain P_2AgO_2 molecular cores with four-coordinate silver in which the carboxylate ligands are weakly bound to the silver atoms *via* the two oxygen atoms giving rise to unsymmetrical chelate units. Crystal structure determinations and solid-state NMR spectra have also been analysed for the mononuclear molecular silver(I) nitrate complex $[(Ph_3P)_2Ag(O_2NO)]$ (**9α)** and two polymorphs of its toluene monosolvate (**11α, β**). In **9α,** the two PPh_3 ligands are of the

same chirality, whereas in **11α, β,** they are opposed. The crystalline environments in the polymorphs have been explored by way of Hirshfeld surface analyses, after quantum-mechanical isolated-molecule calculations had shown that although the molecular energies of the experimental geometries of **9α, 11α, 11β** are significantly different from each other and from the energies of the optimized geometries, the latter, in contrast, do not differ significantly from each other despite the conformational isomerism. It has further been shown using **9α** as an example that the energy dependence on variation of the P-Ag-P angle over a range of *ca* 15º is only *ca* 5 kJ mol^{-1}. All this indicates that the forces arising from crystal packing result in significant perturbations in the experimental geometries, but do not alter the stereoisomerism caused by the donor atom array around the Ag atom. In the NMR study, a strong inverse correlation has been found between $^{1}J(^{107/109}Ag,^{31}P)$ and the Ag-P bond length across all carboxylate and nitrate compounds.

Introduction

The structural versatility of silver(I) in its coordination chemistry has been demonstrated in many studies of its complexes.[1,2] Many of these complexes involve anionic ligands such as halides, pseudohalides and oxyanions. While structural studies of Ag(I) complexes, particularly those of carboxylates, are extensive,[3-10] the importance of such complexes in diverse areas of chemistry justifies extension of this work. E.g., silver carboxylate systems are of considerable interest in a number of different areas of chemistry, such as the synthesis and mechanism of silver metal catalysts, the preparation of silver colloids, nanoparticles and nanowires,[11-20] and antibacterial agents.[21] Silver(I) is known to deactivate cellular enzymes and DNA by coordinating to electron-donating groups such as carboxylates.[22]

Previous studies have characterized examples involving formate, the simplest possible carboxylate ligand, coordinated to silver(I) both by single-crystal X-ray and spectroscopic methods,[5,6] while more recent studies on the related silver(I) triphenylphosphine:carbonate 2:1 complexes have focussed on the $[(Ph_3P)_2Ag(O_2COH)]$, $[(Ph_3P)_2Ag(\mu\text{-}O.CO.OH)_2Ag(PPh_3)_2]$, and $[(Ph_3P)Ag(O,\mu\text{-}O'\cdot CO)Ag(PPh_3)_2]\cdot(2H_2O)$ systems.[23] The present work was intended to provide further structural characterizations of related complexes of the 1:2 type Ag(carboxylate):PPh_3 complexes supporting carboxylate ligands such as phenylacetate ($PhCH_2CO_2^-$, **1**), diphenylacetate ($Ph_2CHCO_2^-$, **2**), *t*-butyrate ($(CH_3)_3CCO_2^-$, **3**) and *t*-butylacetate ($(CH_3)_3CCH_2CO_2^-$, **4**).

Triphenylphosphine PPh_3 can be used as a co-ligand in silver(I) carboxylate complexes to

prevent the formation of O-bridged oligomers or polymers.[20] It also provides an NMR probe in the form of the ^{31}P nucleus, so that ^{31}P CPMAS solid-state NMR spectroscopy may be used to measure heteronuclear $^{1}J(^{107/109}Ag,^{31}P)$ and homonuclear $^{2}J(^{31}P,^{31}P)$ spin-spin coupling constants. These, linked with the relevant X-ray structural data, provide information about the metal-ligand bonding in the complexes, in further extension of the previous carbonate work. Hence, literature-known compounds were re-synthesized and crystallized to allow corresponding solid-state NMR experiments: acetate ($CH_3CO_2^-$) (**6**, unsolvated[24], and **7**, EtOH.H_2O solvate[25]), lactate ($CH_3(HO)CCO_2^-$, **8**),[26] and trifluoroacetate ($CF_3CO_2^-$, **5**)[27]. For the latter, by repeating the single-crystal structure determination experiment, a second phase was identified that we call **5β**. While investigating this polymorphism with Hirshfeld Surface analysis and theoretical calculations, we realised that the isoelectronic nitrate anion forms silver (I) complexes that also exhibit polymorphism (**9α** *vs* **9β** and **11α** *vs* **11β**, Figure 1). Therefore, such complexes were included in the spectroscopic, X-ray diffraction, Hirshfeld surface analysis and solid-state NMR studies; more details in the experimental section.

We further note that the perfluorobutyrate complex $[(Ph_3P)_2Ag(O_2CC_4F_7)]$ has been previously recorded,[28] but a more precise low-temperature measurement was conducted in the course of this work (CCDC 856752). Parallel studies of structures and spectroscopy of a number of relevant copper(I) counterparts are reported in the literature.[29-33]

Experimental and Computational Details

Preparation of compounds

Crystalline samples of the 1:2 silver(I) carboxylate or nitrate complexes with triphenylphosphine described herein were readily obtained in general from the reaction of stoichiometric quantities of the reagents in aqueous ethanol.

$[(Ph_3P)_2Ag(O_2CCH_2Ph)]$, 1. Found: C 68.6, H 4.9; calc. for $C_{44}H_{37}AgO_2P_2$: C 68.85, H 4.86%.

$[(Ph_3P)_2Ag(O_2CCHPh_2)]\cdot$EtOH, 2. Found: C 70.3, H 5.3; calc. for $C_{52}H_{47}AgO_3P_2$: C 70.20, H 5.32%.

$[(Ph_3P)_2Ag(O_2CC(CH_3)_3]$, 3. Found: C 67.2, H 5.4; calc. for $C_{41}H_{39}AgO_2P_2$: C 67.13, H 5.36%.

$[(Ph_3P)_2Ag(O_2CCH_2C(CH_3)_3)]$, 4. Found: C 67.7, H 5.5; calc. for $C_{42}H_{41}AgO_2P_2$: C 67.48, H 5.53%.

$[(Ph_3P)_2Ag(O_2CCF_3)]$, 5. The complex was prepared as described in the literature[27] except for

the use of methanol rather than ethanol as solvent, resulting in the crystallization of a new phase, designated as '**β**', with the earlier being '**α**'.

For the present NMR studies, several known, structurally characterized complexes were prepared following the literature procedures. They are as follows: $[(Ph_3P)_2Ag(O_2CCH_3)]$, **6**[24]; $[(Ph_3P)_2Ag(O_2CCH_3)]\cdot EtOH\cdot H_2O$, **7**[25]; $[(Ph_3P)_2Ag(O_2CC(OH)CH_3)]$, **8**[26], together with the nitrate analogue recorded as mononuclear $[(Ph_3P)_2Ag(O_2NO)]$, **9α**[35], and its triclinic benzene monosolvate[36], **10**. A binuclear form, $[(Ph_3P)_2Ag(\mu\text{-}ONO_2)_2Ag(PPh_3)_2]$, unspecified crystallization solvent, has also been recorded **9β**[37]. In the present work, crystallization from toluene yielded the $[(Ph_3P)_2Ag(O_2NO)]$ toluene mono-solvate, in triclinic, **11α,** and monoclinic, **11β**, forms. Thus, 2.6 g PPh_3 and 0.5 g $AgNO_3$ were stirred in 100 ml boiling toluene. This resulted in only partial dissolution of the $AgNO_3$. The toluene solution was decanted off and the residual $AgNO_3$ dissolved in 5 ml warm acetonitrile. The original toluene solution was added to the acetonitrile solution and the resultant clear solution boiled for 20 min leading to a reduction of the volume to ~ 75 ml. This solution was filtered and let stand in ambient conditions for 6 h. Initially, acicular crystals precipitated (**11β**) which then transformed into well-defined blocks (**11α**). Melting point: 221-224ºC after loss of solvent. Elementary Analysis: Found C 66.7, H 4.9, N 1.65; calc. for $C_{35}H_{30}P_2AgNO_3\cdot C_7H_8$ C 65.66, H 4.87, N 1.78%. Reproducibility of acquisition of the monoclinic (**11β**) form was adventitious.

X-ray Structure determinations

Data were measured on a CCD area-detector diffractometer with monochromatic Mo Kα radiation (λ = 0.71073Å) or Cu Kα radiation (λ = 1.54184Å) in the case of **6**. Following absorption corrections and solution by direct methods, the structures were refined on F^2 using full matrix least squares refinement. Neutral atom complex scattering factors were employed within the SHELXL 97 program.[38] Pertinent results are given below and in Tables S1 and S2 of the Supplementary Material. Figure 1 shows the crystal structures of the polymorphic nitrate complexes **9β, 11α** and **11β**.

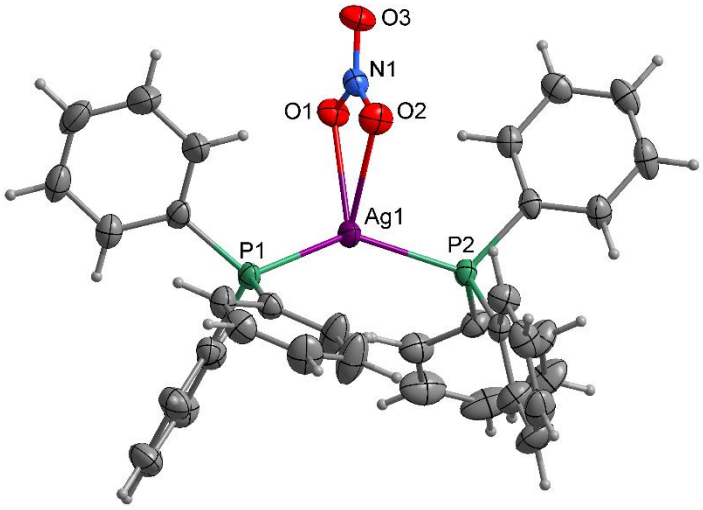

(a)

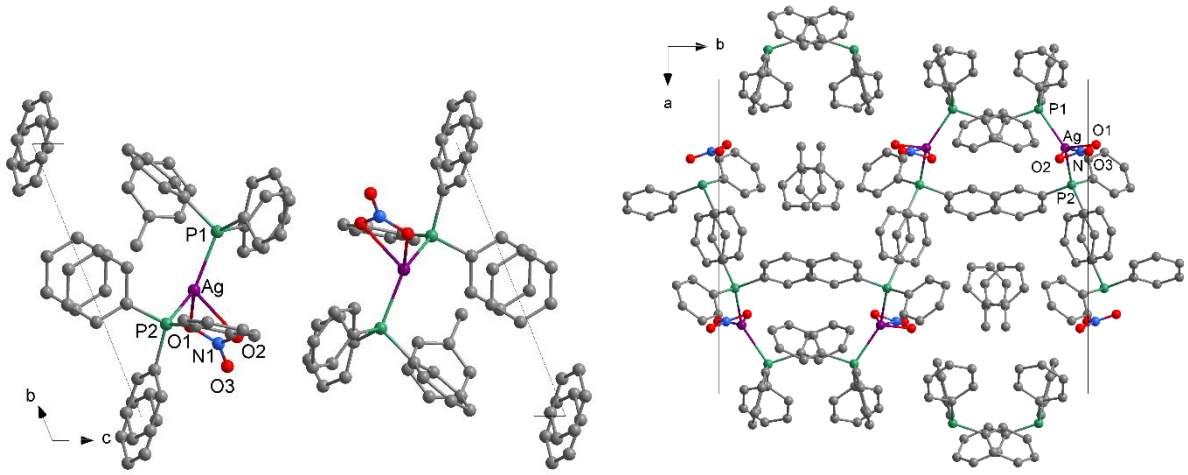

(b) (c)

Figure 1. (a) Molecular projection of unsolvated [$(Ph_3P)_2Ag(O_2NO)$], **9α** (200 K). (b) Unit cell contents of **11α**, projected down *a*, as exemplary of the triclinic form of the toluene mono-solvate which also accommodates the isomorphous benzene mono-solvate (**10**). Hydrogen atoms have been omitted. (c) Unit cell contents of the monoclinic form of the toluene mono-solvate, **11β**, projected down *c*. Hydrogen atoms have been omitted.

[$(Ph_3P)_2Ag(O_2CCH_2Ph)$], 1. $C_{44}H_{37}AgO_2P_2$, *M* 767.6, triclinic, space group $P\bar{1}$ (C_i^1, No. 2), *a* 12.9007(9), *b* 13.0963(9), *c* 13.3198(9) Å, α 66.416(1), β 62.517(1), γ 71.981(1)°, *V* 1808.0(2) Å^3, *T* 168 K, *Z* 2, D_c 1.410 g cm^{-3}. μ_{Mo} 0.68 mm^{-1}, specimen: 0.64 x 0.50 x 0.44 mm, absorption $T_{min/max}$ 0.89, $2\theta_{max}$ 53°, 22760 reflections collected, 7275 unique (R_{int} 0.026). Final *Goof* 0.94, *R1* 0.022, *wR*2 0.056, *R* indices based on 6312 reflections with $I > 2\sigma(I)$, $|\Delta\rho_{max}|$ 0.55 e Å^{-3}. CCDC: 1957300**.**

[(Ph$_3$P)$_2$Ag(O$_2$CCH$_2$Ph)]·EtOH, 2. $C_{52}H_{47}AgO_3P_2$, *M* 889.7, triclinic, space group $P\bar{1}$, *a* 9.5272(7), *b* 10.7687(8), *c* 21.042(2) Å, α 98.260(1), β 89.819(1), γ 89.715(1)º, *V* 2136.4(3) Å^3, *T* 168 K, Z 2, D_c 1.383 g cm^{-3}, μ_{Mo} 0.59 mm^{-1}, specimen: 0.44 x 0.42 x 0.28 mm, absorption $T_{min/max}$ 0.92, $2\theta_{max}$ 52º, 26935 reflections collected, 8457 unique (R_{int} 0.038). Final *Goof* 1.00, *R1* 0.044, *wR*2 0.113, *R* indices based on 6552 reflections with $I > 2\sigma(I)$, $|\Delta\rho_{max}|$ 2.15 e Å^{-3}. CCDC: 1957301.

The ethyl group of the solvent molecule was modelled as disordered over two sets of sites of equal occupancy.

[(Ph$_3$P)$_2$Ag(O$_2$CC(CH$_3$)$_3$)], 3. $C_{41}H_{39}AgO_2P_2$, *M* 733.5, monoclinic, space group $P2_1/n$ (C_{2h}^5, No. 14, variant), *a* 14.689(1), *b* 12.082(1), *c* 20.577(2) Å, β 96.584(1)º, *V* 3627.6(6) Å^3, *T* 168 K, *Z* 4, D_c 1.343 g cm^{-3}, μ_{Mo} 0.68 mm^{-1}, specimen: 0.34 x 0.30 x 0.05 mm; absorption $T_{min/max}$ 0.82, $2\theta_{max}$ 53º, 43157 reflections collected, 7334 unique (R_{int} 0.12). Final *Goof* 1.0, *R1* 0.056, *wR*2 0.130, *R* indices based on 3780 reflections with $I > 2\sigma(I)$, $|\Delta\rho_{max}|$ 1.26 e Å^{-3}. CCDC: 1957305.

The *t*-butyl group was modelled as disordered about its pendant bond, with restrained geometries.

[(Ph$_3$P)$_2$Ag(O$_2$CCH$_2$C(CH$_3$)$_3$)], 4. $C_{42}H_{41}AgO_2P_2$, *M* 747.6, triclinic, space group $P\bar{1}$, *a* 12.5459(9), *b* 14.736(1), *c* 21.252(2) Å, α 97.059(1), β 106.498(1), γ 92.693(1)º, *V* 3724.9(5) Å^3, *T* 168 K, *Z* 4, D_c 1.333 g cm^{-3}, μ_{Mo} 0.66 mm^{-1}, specimen: 0.42 x 0.26 x 0.12 mm; absorption $T_{min/max}$ 0.84, $2\theta_{max}$ 53º; 49244 reflections collected, 15059 unique (R_{int} 0.065). Final *Goof* 0.91, *R1* 0.040, *wR*2 0.086, *R* indices based on 9307 reflections with $I > 2\sigma(I)$, $|\Delta\rho_{max}|$ 0.97 e Å^{-3}. CCDC: 1957307**.**

[(Ph$_3$P)$_2$Ag(O$_2$CCF$_3$], 5β. $C_{38}H_{30}AgF_3O_2P_2$, *M* 745.5. monoclinic, space group *C*2/*c* (C_{2h}^6, No.15), *a* 23.403(1), *b* 12.0965(7), *c* 23.396(1) Å, β 94.044(1)º, *V* 6607 Å^3, *T* 153 K, *Z* 8, D_c 1.499 g cm^{-3}, μ_{Mo} 0.76 mm^{-1}, specimen: 0.18 x 0.13 x 0.10 mm, absorption $T_{min/max}$ 0.87, $2\theta_{max}$ 75º; 68165 reflections collected, 17368 unique (R_{int} 0.076). Final Goof 0.87, *R1* 0.045, *wR*2 0.097, *R* indices based on 8066 reflections with $I > 2\sigma(I)$, $|\Delta\rho_{max}|$ 1.27 e Å^{-3}. CCDC: 856751.

This structure is a new polymorph, *cf.* the previously recorded orthorhombic *Pbca* form, designated 'α'.[27] The fluorine atoms were modelled as rotationally disordered over two sets of sites, occupancies refining to 0.682(7) and complement.

$[(Ph_3P)_2Ag(O_2NO)]$, 9α. $C_{36}H_{30}AgNO_3P_2$, *M* 694.4, triclinic, space group $P\bar{1}$, *a* 11.7453(5), *b* 11.9791(6), *c* 13.5588(6) Å, α 102.613(4), β 112.017(4), γ 105.338(4)º, *V* 1594.4(2) Å^3, *T* 200 K, *Z* 2, D_c 1.446 g cm^{-3}, μ_{Mo} 0.77 mm^{-1}, specimen: 0.39 x 0.28 x 0.18 mm, absorption $T_{min/max}$ 0.86, $2\theta_{max}$ 55º, 11407 reflections collected, 7288 unique (R_{int} 0.016). Final Goof 0.96 *R1* 0.024, *wR*2 0.056, *R* indices based on 6128 reflections with $I > 2\sigma(I)$, $|\Delta\rho_{max}|$ 0.47 e Å^{-3}. CCDC: 764196. See Figure 1 (a).

Room-temperature studies have been previously recorded;[35(a,b)] a determination has also recently been recorded at 120 K.[35(c)]

$[(Ph_3P)_2Ag(O_2NO)]\cdot C_7H_8$, 11. $C_{43}H_{38}AgNO_3P_2$, *M* 786.6.

Triclinic form, 11α. Space group $P\bar{1}$, *a* 11.2434(4), *b* 12.3381(6), *c* 16.2534(6) Å, α 106.398(4), β 96.842(3), γ 115.208(4)º, *V* 1881.1(2) Å^3, *T* 200 K, *Z* 2, D_c 1.389 g cm^{-3}, μ_{Mo} 0.66 mm^{-1}, specimen: 0.47 x 0.45 x 0.43 mm, absorption $T_{min/max}$ 0.98, $2\theta_{max}$ 55º, 15664 reflections collected, 8608 unique (R_{int} 0.019). Final Goof 1.05, *R1* 0.027, *wR*2 0.067, *R* indices based on 7366 reflections with $I > 2\sigma(I)$, $|\Delta\rho_{max}|$ 0.57 e Å^{-3}. CCDC: 764197. This form is isomorphous with the previously recorded benzene solvate (**10**), see also Figure 1 (b).[36]

Monoclinic form, 11β. Space group $P2_1/c$, *a* 16.637(2), *b* 19.265(4), *c* 12.1100(13) Å, β 102.661(9) º, *V* 3787.0(10) Å^3, *T* 295 K, *Z* 4, D_c 1.380 g cm^{-3}, μ_{Mo} 0.66 mm^{-1}, specimen: 0.30 x 0.20 x 0.10 mm, absorption $T_{min/max}$ 0 94, $2\theta_{max}$ 50º, 6667 reflections collected. Final Goof 0.98, *R1* 0.077, *wR*2 0.209, *R* indices based on 3408 reflections with $I > 2\sigma(I)$, $|\Delta\rho_{max}|$ 2.1 e Å^{-3}. CCDC: 764198. A unique data set was measured on a capillary mounted specimen using a single counter instrument; a gaussian absorption correction was applied. See Figure 1 (c).

^{31}P MAS NMR Spectroscopy

Solid state ^{31}P CPMAS NMR data were obtained at ambient temperature on a Bruker DSX-400 (9.40 T) spectrometer operating at a ^{31}P Larmor frequency of 161.92 MHz. Conventional cross-polarization[39] and magic-angle-spinning[40] techniques, coupled with spin temperature alternation[41] to eliminate spectral artefacts, were implemented using a Bruker 3.2 mm double-air-bearing probe in which MAS frequencies of ~10-12 kHz were achieved. An initial ^{1}H $\pi/2$ pulse width of 3 μs, recycle delay of 15 - 30 s, Hartmann-Hahn contact period of 2 - 5 ms and a ^{1}H decoupling field of 80 - 85 kHz (during acquisition) were used in these ^{31}P experiments. The reported ^{31}P chemical shifts were externally referenced to the IUPAC standard of 85% H_3PO_4 via a secondary solid reference of ammonium dihydrogen phosphate ($(NH_4)(H_2PO_4)$) which exhibits a shift of δ 1.0 ppm; this secondary reference material was also used to set the Hartmann–Hahn condition. The 2D homonuclear ^{31}P-^{31}P CPCOSY experiment was implemented with the TPPI (time proportional phase incrementation) method[42–44] for acquisition of phase-sensitive data in both the F1 and F2 dimensions. The application of this technique has been discussed in detail elsewhere.[45] The recycle delay, contact period, ^{1}H $\pi/2$ pulse width and MAS rate were the same as those implemented in the above 1D ^{31}P CPMAS experiments. A total of 256 F1 increments were acquired into 256 word locks, with both dimensions zero-filled to 1 K words and weighted with Gaussian multiplication prior to Fourier transformation.

Theoretical calculations

Experimental geometries taken from the crystallographic data files (CIFs) were used as input for electronic energy calculations to assess the relative energy separations between the forms **9α**, **11α**, **11β**. The PW6B95 hybrid functional was used,[46] as implemented in the ORCA program suite.[47] This particular functional was used as it was found to perform exceptionally well in a large-scale bench-marking exercise, concerning basic properties, reaction energies, and non-covalent interactions.[48]

The complexes were modelled using the cc-pvdz basis set for hydrogen, carbon, nitrogen, oxygen, and phosphorus.[49,50] To reduce the size of the calculation, an effective core potential was implemented for silver, being the cc-pvdz PP basis set.[51] This PP basis set accounts for relativistic effects for the heavier silver atom and consists of small-core relativistic pseudopotentials adjusted to multiconfiguration Dirac-Hartree-Fock data based on the Dirac-Coulomb-Breit Hamiltonian.

Calculations were performed on the fixed experimental geometries transferred from the solid state into the isolated state, and, additionally, geometry optimisations were carried out. Initial optimisations were carried out using the 6-31G basis set for C,H,N,O, and P and cc-pvdz PP for Ag, and these were followed by the cc-pvdz basis set calculations. Following on, vibrational frequency calculations were undertaken to ensure that the converged geometry in each case was a minimum on the global potential energy surface.

Hirshfeld Surface analyses

The Hirshfeld Surface ('HS') approach[52-56] as implemented in the programme CrystalExplorer[52] offers useful insight into the environments of the molecules in a number of the above related forms. A Hirshfeld Surface is the outer contour of the space ascribed to a molecule or an atom in a crystalline environment. It can be compared to a van-der-Waals envelope that other molecules or atoms come into contact with when interactions are present. The directions and strengths of these interactions can be mapped onto the HSs using various descriptors such as 'curvedness of the surface'[54] and 'd_{norm}'[55]. The latter is a ratio encompassing the distances of any surface point to the nearest interior (d_i) and exterior (d_e) atoms and the van-der-Waals radii of the atoms.[55] Also of use is a plot of d_i *vs* d_e, referred to as a 'fingerprint plot', which identifies the occurrence of different kinds of interactions.[56] These have been successfully used to explore polymorphism.[57] In particular, it has been shown that compounds which were claimed to be polymorphic in fact belong to the same modification consequent on fingerprint plots revealing identical chemical environments. This technique has been applied to those structures found to exhibit polymorphism in the present work in an effort to better understand the factors governing their appearance.

Results and discussion

Crystal structures

The structures of the monocarboxylic acid complexes **1-4**, **5β**, may be described as neutral mononuclear molecular forms $[(Ph_3P)_2Ag(O_2CR)](\cdot S)$. In the case of $R = CH_2C(CH_3)_3$, (**4**), two molecules rather than one comprise the asymmetric unit of the structure, but all are in centrosymmetric space groups. The descriptors of the full array of P_2AgO_2 coordination environments recorded in Table S1 (Supplementary Material) are generally widely scattered across the full suite of compounds recorded therein (*i.e.* **1-8**), Ag-P ranging between 2.4063(8) and 2.4671(9) Å, with differences as great as 0.05 Å within one compound (**7**). Ag-O range

between 2.379(3) and 2.542(4) Å (excepting one 'outlier' value (2.894(4) Å) within the present trifluoroacetate (**5β**) determination). Interestingly, polymorph **5α** (orthorhombic *Pbca*)[27], with a closely symmetrically chelating carboxylate group, has a remarkably large P-Ag-P angle (142.18(4)º), which is more usual (129.35(5)º) in the unsymmetrically chelated polymorph **5β**. However, in consequence of the carboxylate asymmetry, **5β** has an unusually small O-Ag-O angle (47.18(9)°). There are no unusually close additional Ag...O intermolecular interactions. Among the previously determined structures of **5α, 6-8**, two molecules comprise the asymmetric units in the cases of **6** and **7**. It is of interest that in the solvates of **2**(·EtOH) and **7**(·EtOH·H_2O),[25] there are no close solvent-O...Ag interactions. In contrast, in the structures of their copper(I) analogues [$(Ph_3P)_2Cu(O_2CCH_{(0,1)}F_{(3,2)})$]·EtOH the ethanol molecules are strongly *O*-coordinated so that the carboxylate becomes monodentate therein, thus [$(Ph_3P)_2Cu(O.CO.CH_{(0,1)}F_{(3,2)})(HOEt)$].[32] Neither of the present polymorphs of **5** is isomorphous with the copper(I) analogue [$(PhP_3)_2Cu(O_2CCF_3)$],[32] although the latter is isomorphous with its acetate counterpart [$(Ph_3P)_2Cu(O_2CCH_3)$],[31] that in turn not being isomorphous with its silver(I) analogue[24] (Table S2, Supplementary Material).

$AgNO_3$: PPh_3 (1:2) is isoelectronic with $AgHCO_3$: PPh_3 (1:2). The latter, as discussed in the Introduction, is found in two forms - mononuclear [$(Ph_3P)_2Ag(O_2COH)$] and binuclear [$(Ph_3P)_2Ag(\mu\text{-}O\cdot CO\cdot OH)_2Ag(PPh_3)_2$]. The nitrate (**9**) is also found in two parallel forms: (a) Binuclear [$(Ph_3P)_2Ag(\mu\text{-}O\cdot NO_2)_2Ag(PPh_3)_2$], (**9β**),[37] surprisingly being isomorphous with the binuclear bicarbonates of both silver(I)[23] and copper(I)[29] (Table S2), in which intermolecular hydroxylic hydrogen bonds are present and significant in the description of the structure. (b) Mononuclear [$(Ph_3P)_2Ag(O_2NO)$], (**9α**, see Figure 1 (a)), the latter the subject of two earlier determinations at room temperature,[35(a,b)] and another at 120 K.[35(c)] It has also been described as a mononuclear form, which is a benzene monosolvate (**10**).[36] The unsolvated form is not isomorphous with its *O,O'*-nitrito analogue (*P*2/*c*)[58] nor with the copper(I) nitrite[59] or nitrate[60] form (both isomorphous, *C*2/*c*) (Table S2).

The results of the structure determinations of the two phases of the 1:2 adduct of silver(I) nitrate with triphenylphosphine, as crystallized from toluene, are consistent with a description in terms of that stoichiometry: both are mononuclear and solvated with a single molecule of toluene, a single formula unit, devoid of crystallographic symmetry, comprising the asymmetric unit of the structure in each case. In each case, the nitrate is *quasi*-symmetrically *O,O'*-bidentate, thus [$(Ph_3P)_2Ag(O_2NO)$](·C_7H_8). The triclinic form (**11α**, Figure 1 (b)) is isomorphous with the previously described benzene solvate (**10**);[36] the monoclinic form,

accessed adventitiously, is new (**11β**, Figure 1 (c)). A redetermination at 200 K of the structure of the previously described unsolvated mononuclear form,[35] **9α**, provides data of enhanced precision for comparison. Ag-P distances in **9α, 10, 11α,β** range between 2.411(3)-2.4491(5) Å and are similar to those of the carboxylates, but somewhat less diverse, while the more weakly bound Ag-O (2.4287(14)-2.6711(14) Å) are perhaps more widely spread (Table S1). Despite these divergences, the P-Ag-P angles are appreciably greater than in the carboxylate family, all lying above 135.85(9)º, consistent with the greater carboxylate basicity. In all of the nitrate structures, the disposition of the three phenyl groups of each triphenylphosphine ligand adopts the common *quasi*-threefold symmetric disposition, albeit highly distorted, with Ag-P-C-C torsion angles ranging between 9.4(2) and 70.1(2)º (Table 1). However, it is of interest that in **5α,β** and **9α**, the two ligands are of the same chirality, whereas in **10** and **11α,β** they are opposite (Table 1).

Table 1. PPh_3 torsion angles (degrees) in the polymorphic $[(Ph_3P)_2Ag(O_2XY)]$ systems. Angles Ag-P-C-C (|| < 90º) are cited for the three rings of each ligand. *Values* in parentheses are derivative of the 6-31G basis set geometry optimization calculations, while those in parentheses and bold font are for cc-pvdz basis set calculations.

Compound	Ligand 1	Ligand 2
5α (trifluoroacetate)[a]	–51.0(4), –34.2(4), –48.4(4)	–67.0(4), –28.8(4), –21.0(4)
5β (trifluoroacetate)	–38.9(2), –39.3(2), –68.4(2)	–28.5(2), –30.6(2), –46.7(2)
9α (nitrate)	–32.8(2), –44.7(2), –30.5(3)	–9.4(2), –36.0(2), –58.9(2)
	(–29.5) (–36.0) (–20.1)	*(–0.7) (–56.0) (–35.4)*
	(-23.6) (36.4) (-57.4)	***(-25.3) (-15.7) (-37.3)***
10 (nitrate)[b]	16.0(2), 66.1(2), 23.4(2)	–45.1(2), –47.5(3), –41.6(3)
11α (nitrate)	15.4(2), 70.1(2), 20.7(2)	–45.8(2), –45.2(2), –42.9(2)
	(34.7) (26.7) (29.8)	*(–9.6) (–50.1) (–44.9)*
	(35.8) (25.6) (39.7)	***(9.5) (-78.3) (-35.7)***
11β (nitrate)	35.2(9), 57.9(8), 52.0(9)	–29.0(10), –21.3(9), –52.9(8)
	(-24.7) (-30.3) (-36.1)	*(8.6) (43.7) (52.5)*
	(-30.1) (-34.4) (-42.2)	***(0.1) (40.5) (62.0)***

[a] Ref. [27]; [b] ref. [36]. Chiralities for **11β** are the opposite of those of the CIF settings to assist comparison.

In the nitrate forms (**9, 10, 11α, 11β**), there is relatively little variation among the Ag-P distances and the P-Ag-P angles (Table S1), despite the polymorphism of **11** and the differences in the ligand chiralities therein. By contrast, considerable divergences are found in the P-Ag-P angles (142.18(4), 129.35(5)º) for the trifluoroacetates **5α**, **5β** in which the pairs of ligand chiralities are the same. Comparison of the present results with those of similar copper(I) compounds (Table S1) shows a contracted coordination sphere in the latter *vs.* the former, with no consistent demarcation between the P-Cu-P angles in respect of carboxylate *vs.* nitrate.

Crystal architecture considerations

The present array of determinations is interesting in respect of the groups of polymorphs and isomers uncovered here and in related studies (Table S2).

(a) $[(Ph_3P)_2Ag(O_2CCF_3)]$ (**5**) now is defined in two forms: orthorhombic *Pbca* (**5α**)[27] and monoclinic *C*2/*c* (**5β**), both centrosymmetric with one mononuclear molecule in the asymmetric unit. Neither is isomorphous with $[((Ph_3P)_2Ag(O_2CCH_3)]$ or $[(Ph_3P)_2Cu(O_2CCF_3)]$, although the latter is isomorphous with $[(Ph_3P)_2Cu(O_2CCH_3)]$.

(b) $AgNO_3$: PPh_3 (1:2) is found as two isomers: (i) Mononuclear $[(Ph_3P)_2Ag(O_2NO)]$, (**9α,** Figure 1), isoelectronic but not isomorphous with $[(Ph_3P)_2Ag(O_2COH)]$,[23] the space group being centrosymmetric with one molecule in the asymmetric unit. (ii) Binuclear/dimeric $[(Ph_3P)_2Ag(O.NO.O)_2Ag(PPh_3)_2]$, (**9β**),[36] isomorphous with $[(Ph_3P)_2M(O.CO.OH)_2M(PPh_3)_2]$ (M = Cu,[29] Ag[23]) in the unusual noncentrosymmetric space group $P2_12_12$, a two-fold crystallographic axis passing through the centre of the $M(\mu\text{-}O)_2M$ ring.

(c) $[(Ph_3P)_2Ag(O_2NO)]\cdot S$, S = toluene, has been defined in two forms, triclinic and monoclinic, **11α,β** as above (Figure 1), each one centrosymmetric with one mononuclear formula unit in the asymmetric unit, the triclinic form being isomorphous with the previously determined S = benzene solvate (**10**).[36]

Figs. 3(a,b) show the fingerprint plots derivative of Hirshfeld Surfaces for the molecules of **5α** and **5β**, confirming their consistency with different interaction networks within their environments because the overall shapes of their fingerprint plots differ. Both forms exhibit close H...H and C-H...F contacts, with **5β** exhibiting slightly shorter C-H...O contacts than **5α** as well as additional C-H…C contacts (signifying C-H...π interactions) between the phenyl groups. The most distinctive difference between the two modifications is a remarkably short intermolecular C-H...Ag approach in **5α** which is absent in **5β**. Examination of the fingerprint plots resulting from the HS of just the central silver atom (Figs. 3(c,d)), shows that, as well as the Ag-P and Ag-O bonds, the Ag...H contact (2.83Å) is also represented by a distinct feature in the plot of **5α**.

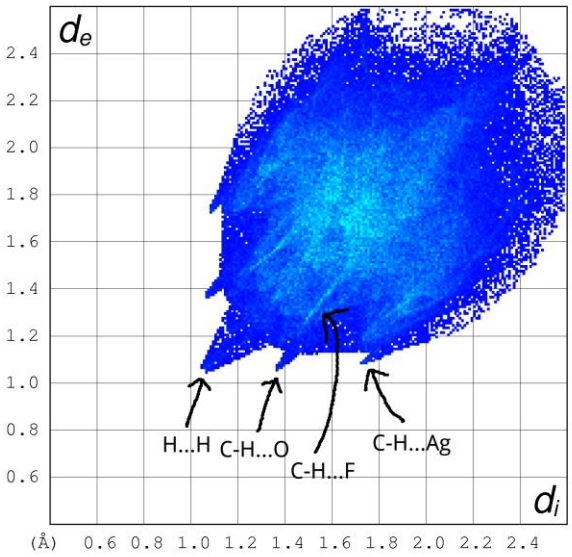

a)

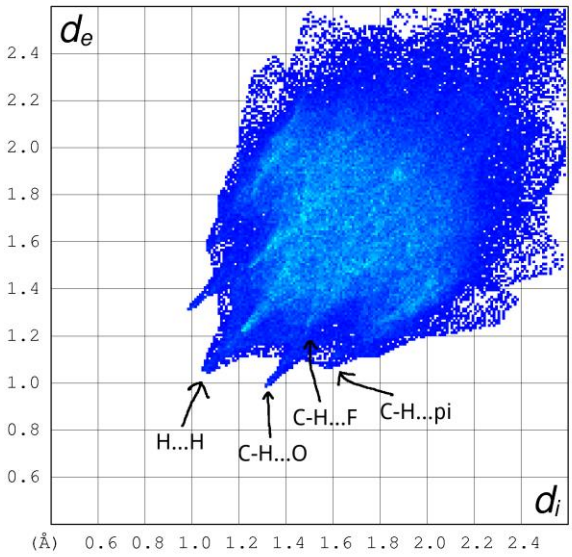

b)

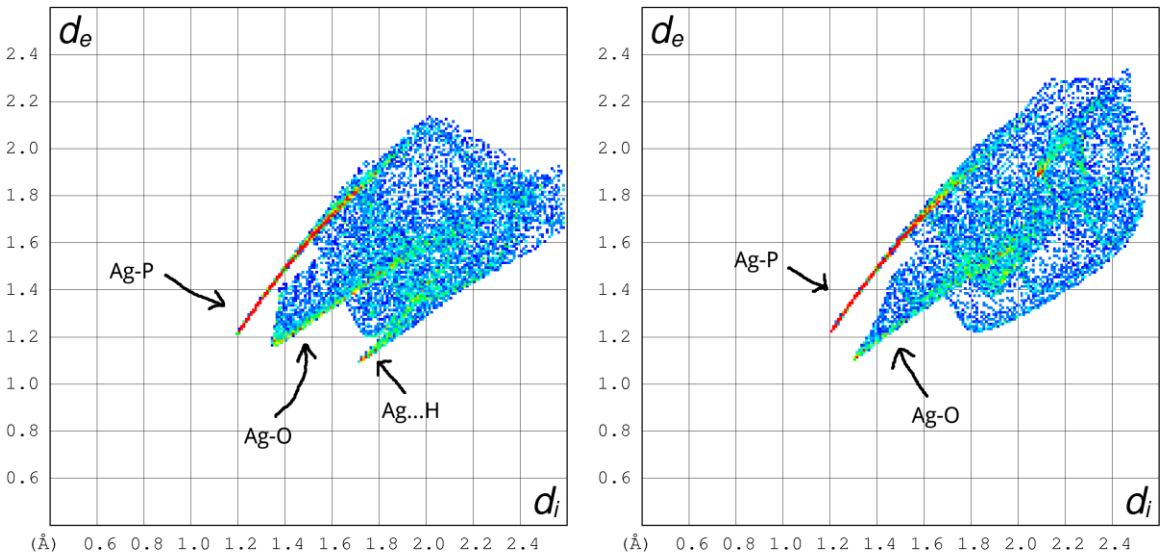

Figure 2. Fingerprint plots with highlighted types of close interactions for the complete coordination complex of a) **5α** and b) **5β** as well as the Ag atom in c) **5α** and d) **5β.**

Table S1 shows the two Ag-O distances to be similar in **5α** (2.526(3) and 2.542(4)Å) but significantly different in **5β** (2.420(3) and 2.894(4)Å). This is reflected not only in the form of the features representing the Ag-O bonds in the fingerprint plots of Figures 2 (c,d), but also in the size and intensity (shown by colour) of the imprint of the second oxygen atoms on the atomic HSs (Figures 3(a,b)). To facilitate comparison, the oxygen atom closer to the silver atom has been drawn with a bond to the silver atom in each case, the further oxygen without. In **5α**, the sizes and intensities of the imprints of both oxygen atoms are very similar, whereas that of the second oxygen atom in **5β** is significantly smaller and less intensive.

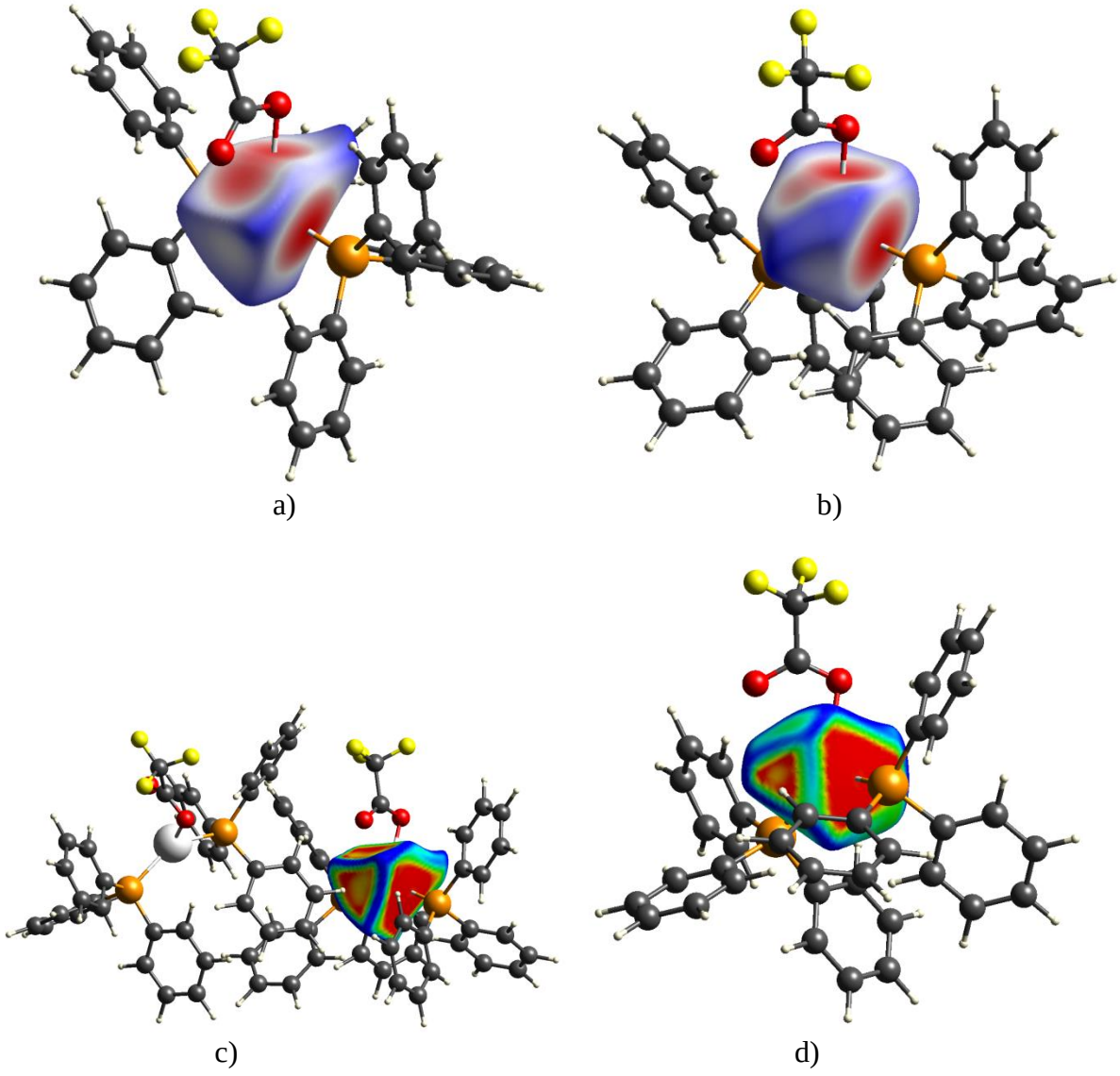

Figure 3. Hirshfeld surfaces of the central silver atom. a) **5α**, d_{norm} plotted onto the surface, scale from red over white to blue (-0.62 to 1.18Å), b) **5β**, d_{norm} plotted onto the surface, scale from red over white to blue (-0.61 to 1.06Å), c) contact pair of **5α**, curvedness plotted onto the surface, scale from red (flattest regions) over yellow and green to blue (most curved regions), d) **5β**, curvedness plotted onto the surface, scale from red (flattest regions) over yellow and green to blue (most curved regions).

The shapes of the HSs of the silver atoms also differ significantly between **5α**, which exhibits a prolonged shape encompassing a contact site to a neighbouring molecule, and **5β**, which has a rather compact shape where the ligands shield the silver atom from the environment. Using the curvedness of the HS itself as the map property (Figures 3(c,d)), each

contact site can be described by a contact patch, a flattened region of the HS bounded by curved regions (blue colour). Figure 3(c) shows that the contact patch directed towards the crystalline environment in **5α** is the above discussed C-H...Ag interaction. However, Figure 3(d) shows that **5β** also exhibits a C-H...Ag interaction. It is an intramolecular or agostic interaction whose contact patch on the silver HS is significantly smaller than that of the intermolecular one in **5α**, with a contact distance 0.22Å longer than the one in **5α**. This agostic interaction in **5β** shields the silver atom from the environment and is the main distinguishing feature between the two forms. The large P-Ag-P angle in **5α** (see Table S1) is a concomitant of the occurrence of the intermolecular C-H...Ag contact, whereas the intramolecular C-H...Ag contact in **5β** only becomes possible with a much smaller P-Ag-P angle. Moreover, the quite different conformations of the ligands in **5α** and **5β** (see the torsion angles presented in Table 1) are concomitants of the different C-H..Ag contacts.

For all of the shown fingerprint plot and HS representations of compound **5**, only one orientation of the major component of the disordered trifluoromethyl group (both phases) has been considered, there being virtually no difference when the other of the two resolvable orientations is used.

The three structures of the unsolvated (**9α**) and toluene-solvate forms (**11α, 11β**) of the nitrate coordination complexes are intriguing in their difference regarding the relative chiralities of the pair of triphenylphosphine ligands. This matter was pursued further by consideration of their relative energies and the nature of their interactions, the subject of an earlier related study.[61] With conformations as found in their crystal lattices, molecular isolated **9α** was found to be the lowest energy form, the separations being large enough to be significant (Table 2).

Table 2. Relative energies (ΔE) of **9α, 11α, 11β** with confirmations as found in their crystal lattice and *optimized isolated molecule* geometries (cc-pvdz basis set calculations). For the optimized geometries, zero point energy corrected differences are reported (ΔE_{zpe}).

Structure	SPE*/Hartree	ZPE**/ kJ·mol^{-1}	ΔE/kJ·mol^{-1}	ΔE_{zpe} /kJ.mol^{-1}
9α	-2504.954177		0	-
	-2505.466300	*1498*	*11*	*11*
11α	-2504.943015		29	-
	-2505.470424	*1497*	*0*	*0*
11β	-2504.882174		189	-
	-2505.468550	1498	*5*	*6*

*Single Point Energy, **Zero Point Energy

After allowing the molecules to relax to their gas phase optimized geometries, the ordering has changed, following a noticeable change in the geometry of the **9α** structure, with the energy separations greatly diminished between the three molecules, including both stereoisomeric forms (Table 2). Thus, the stereoisomerism, at least in the isolated case where there are no interactions with other chiral molecules, is not associated with any appreciable energy difference. The energy differences among the experimental geometries (Table 2) thus presumably arise from conformational perturbations induced by crystal packing forces. This matter was also explored further by examination of the interactions within the crystal lattices using the Hirshfeld Surface (HS) approach.

Before doing so, a final note is in order concerning the theoretical calculations. As discussed above, in respect of their experimental geometries (Table S1), very significant differences are evident, not only between complexes of different anions (carboxylate *vs.* nitrate), but also within those of the same anion (*e.g.* the two phases of the trifluoroacetate

5α,β). It is therefore debatable whether observed differences in particular in angular geometries, most notably in respect of P-Ag-P angles, which are consistently contracted in the optimized situation (Table 3), are consequent on changes in the molecular ambience (*e.g.* **5α**) or deficiencies in the wavefunctions employed. Exigencies in computation costs do not permit further comprehensive pursuit of this dimension of the problem at this stage, and we set it aside for possible future study. However, as a more limited exercise, we have sought to explore the susceptibility of the P-M-P to variations, and have produced a one-dimensional potential energy curve to estimate the change in energy along this coordinate for **9α** as a representative complex. Constrained geometry optimisations were undertaken with the P-Ag-P angle set to values between that observed in the crystal structure (138.58(1)º) and the angle predicted from the fully optimised gas-phase calculation (123.8º). Values for the energies are presented in Table 4, together with consequent Ag-P distances. As can be readily seen, there is only a 5 $kJ{\cdot}mol^{-1}$ energy difference between the maximum of the curve (corresponding to the crystal P-Ag-P angle) and the minimum (corresponding to the fully optimised gas phase P-Ag-P angle). The small energy difference indicates that the interactions of the complex with near neighbours in the crystal phase, and subsequent absence in the gas phase, can easily account for the change in P-Ag-P here and, presumptively more widely among the present and related complexes, **9α** being a representative example.

Table 3. Selected geometries for **9α, 11α, 11β**. The three values in each entry are experimental, *theoretical* (6-31G) and ***theoretical*** (cc-pvdz), respectively.

	9α (1028)	**11α** (1027)	**11β** (194)
Distances (Å)			
Ag-P(1)	2.4391(5), *2.423*, ***2.370***	2.4232(5), *2.412*, ***2.404***	2.430(2), *2.457*, ***2.396***
Ag-P(2)	2.4360(5), *2.437*, ***2.410***	2.4366(5), *2.452*, ***2.400***	2.411(3), *2.418*, ***2.395***
Ag-O(1)	2.4551(13), *2.335*, ***2.322***	2.468(2), *2.337*, ***2.306***	2.451(7), *2.336*, ***2.320***
Ag-O(2)	2.6431(16), *2.438*, ***2.430***	2.550(2), *2.492*, ***2.436***	2.541(7), *2.495*, ***2.438***
Angles (degrees)			
P(1)-Ag-P(2)	138.58(1), *119.4*, ***123.8***	138.10(2), *124.2*, ***117.6***	135.85(9), *123.8*,***122.2***
P(1)-Ag-O(1)	110.96(3), *125.5*, ***128.2***	114.08(4), *118.4*, ***123.9***	109.9(2). *117.1*, ***116.9***
P(1)-Ag-O(2)	100.11(3), *113.4*, ***107.9***	110.68(4), *127.0*, ***105.5***	98.4(2), *90.3*,*107.6*
P(2)-Ag-O(1)	109.99(3), *112.2*, ***110.0***	107.35(4), 117.0,**118.6**	113.7(2), *118.7*,*120.9*
P(2)-Ag-O(2)	101.07(3), *111.6*, ***104.3***	99.60(4), *90.8*, ***109.2***	114.5(2), *127.5*,***105.3***
O(1)-Ag-O(2)	50.26(4), *55.5*, ***54.1***	51.31(5), *54.7*, ***54.3***	50.5(2), *54.7*, ***54.1***

Table 4. Estimated variation of energy *vs* P-Ag-P angle (Ag-P optimized) in **9α** (see text)

Angle (degrees)	Ag-P (Å)	Energy (hartree)	ΔE ($kJ \cdot mol^{-1}$)
123.8	2.370, 2.410	-2505.466300	0.0
128.6	2.357, 2.405	-2505.465931	1.0
133.0	2.354, 2.363	-2505.465625	1.8
138.6	2.363, 2.405	-2505.464274	5.3

In Figure 4, fingerprint plots for the mononuclear complex $[(Ph_3P)_2Ag(O_2NO)]$ molecule in its four different forms are shown. The plots for the isomorphous benzene (**10**) and toluene (**11α**) solvates (Figures 4(b,c)) are very similar as might be expected, whereas the plots for the polymorphic toluene solvates (**11α** and **β**) are quite different from each other (Figures 4(c,d)), and, in turn, different from that of the unsolvated form **9α** (Figure 4(a)). These confirm that in

total three different chemical environments are present among the four different forms of crystalline [$(Ph_3P)_2Ag(O_2NO)$]. All forms exhibit H...H and C-H...O approaches in their crystal packing network, which are much more pronounced for **9α** and **11β**. In these, the H...H approaches are very close, particularly so in **11β** with the shortest H...H intermolecular distance being about 2.0Å. The isomorphic **10** and **11α** possess both weak C-H...π and π...π interactions (π...π interactions signified by close C…C contacts), whereas **9α** exhibits only very weak π...π and **11β** quite strong C-H...π interactions.

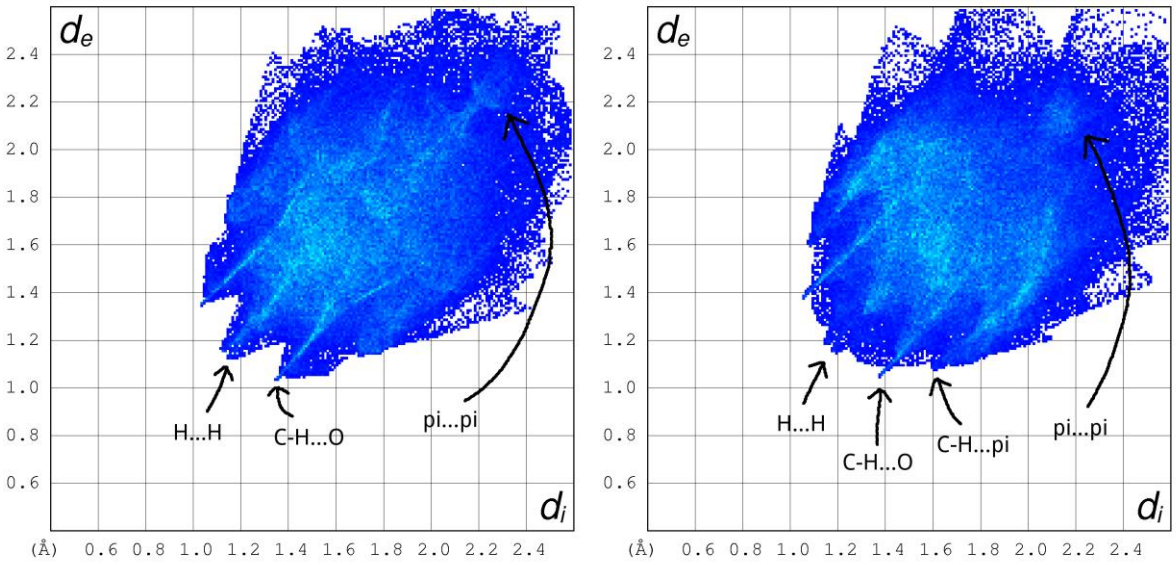

a)

b)

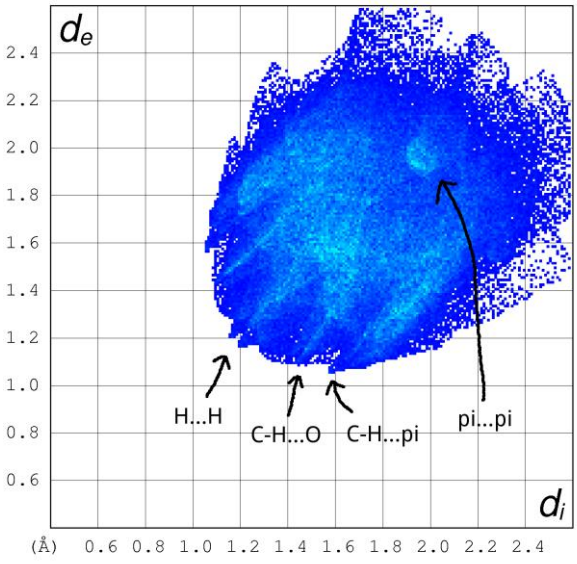

c)

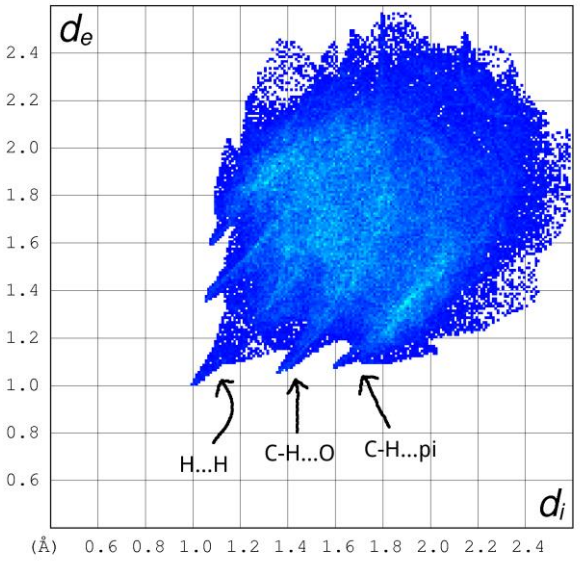

d)

Figure 4. Fingerprint plots with highlighted types of close intermolecular interactions for the complete coordination complex of a) **9α**, b) **10**, c) **11α**, and d) **11β**.

The coordination spheres of the silver atoms are depicted in Figure 5 for **9-11** using the property curvedness plotted onto the HSs. The Ag...O distances are not as divergent as in **5β**, so that there are similarly sized contact patches in all forms investigated here. Moreover, all of the atomic HSs show contact areas arising from their environments; in other words, none of the silver atoms is shielded as in **5β**. Despite their similarities, the shapes of the HSs of the silver atoms are still notably different in the three different environments (**9α** *vs* **10** and **11α** *vs* **11β**), especially with respect to that side which is directed towards the environment. There is a close intermolecular Ag...O approach (3.05 Å) in **9α** (Figure 5(a)), associated with a large, slightly concave contact patch on the atomic HS.

In **10** and **11α**, the crystal packing is significantly different to that in **9α** with the solvate molecules, benzene or toluene respectively, not being involved in any notably close approaches to the substrate molecules. In this packing mode, one phenyl group of a symmetry-related molecule approaches the silver atom of the parent molecule closely, so that two quite weak C-H...Ag interactions occur. They cause a convex contact patch with two small individual imprints (red colour) on the atomic silver HS (Figures 5(b,c)), which differ slightly between **10** and **11α**, with the Ag...H distances 3.27, 3.58Å in **10**, but 3.14, 3.37Å in **11α**. The C-H...Ag contact pattern in **11β** is similar to that in **10** and **11α**, with Ag...H distances 3.03, 3.74Å. It is clear from Figure 5(d) that the closer contact dominates the interaction to the silver atom since there is only one individual imprint (red colour) on the contact patch.

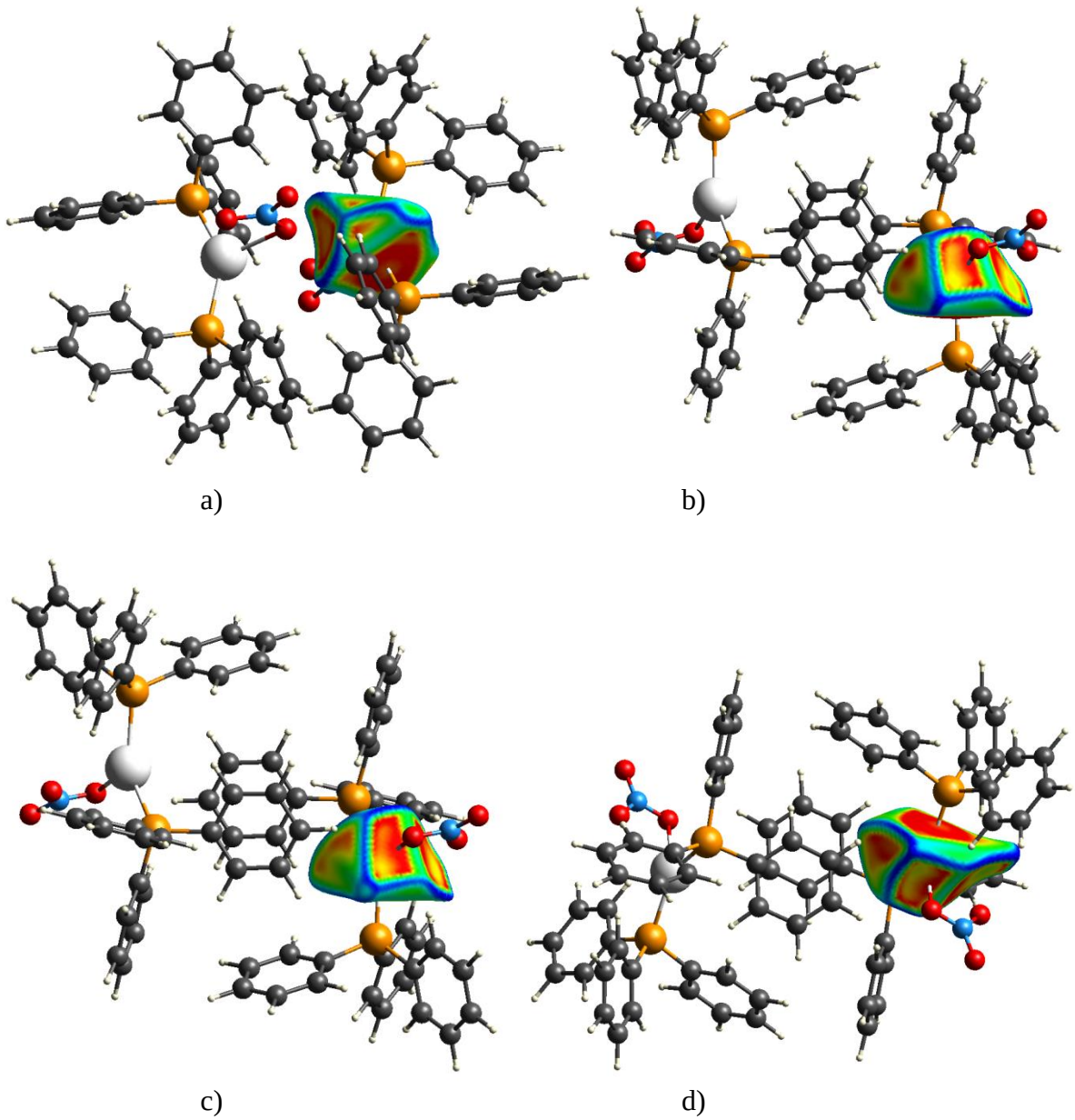

Figure 5. Curvedness plotted onto the Hirshfeld surfaces of the central silver atom, scale from red (flattest regions) over yellow and green to blue (most curved regions) for a) **9α**, b) **10**, c) **11α**, and d) **11β**.

Solid state NMR spectroscopy

The solid state 2D homonuclear ^{31}P-^{31}P CPCOSY MAS NMR data of representative complexes **1**, **2**, **3**, **4**, **5β**, **9α**, **11α** and **11β** are shown in Figure 6, with the corresponding 1D ^{31}P CPMAS NMR spectra being presented as the F1 and F2 projections in these 2D data. All initial NMR parameters elucidated from these measurements have been refined by simulation of the 1D ^{31}P CPMAS spectra and are reported in Table 5. It has been previously established that these 1D ^{31}P CPMAS and 2D ^{31}P-^{31}P CPCOSY MAS NMR data represent ^{31}P chemical shifts resulting from the chemically inequivalent P positions bound to each Ag centre. Each multiplet (doublet) exhibits $^{1}J(^{107,109}\text{Ag},^{31}\text{P})$ scalar coupling between the ^{31}P (I = 1/2) and ^{107,109}Ag (I = 1/2) nuclei, with additional splitting of these doublets (into doublets-of-doublets/quartets) being facilitated via longer-range $^{2}J(^{31}\text{P},^{31}\text{P})$ coupling.[6,9,26,62,63] Each ^{31}P CPMAS spectrum represents the AB portion of an ABX spin system with the strength of the AB coupling being dependent on the ^{31}P chemical shift separation ($\Delta\delta$) of the multiplets. As shown in Figures 6(g) and 7 for $[(PPh_3)_2AgNO_3]$ **9α**, the quartet structure is overlapping and the strong AB coupling scheme necessitates simulation of this multiplet structure to ascertain accurate measurements of the $^{1}J(^{107,109}\text{Ag},^{31}\text{P})$ values.[62] All complexes in this suite have been simulated in this fashion and the results are summarized in Table 5; the remaining simulations being presented in the Supplementary Material (Figure S2). In the cases of the trifluoroacetate **5β** and the nitrate **9α, 11α** and **11β** systems which possess aprotic pendant groups, the homonuclear ^{1}H-^{1}H dipolar network is diminished and the residual ^{31}P MAS linewidths are sufficiently narrow to enable partially resolved $^{1}J(^{107}\text{Ag},^{31}\text{P})$ and $^{1}J(^{109}\text{Ag},^{31}\text{P})$ couplings to be observed (see the data shown in Figure 6). In these cases, only average values of these $^{1}J(^{107}\text{Ag},^{31}\text{P})$ and $^{1}J(^{109}\text{Ag},^{31}\text{P})$ couplings are reported in Table 5 (i.e. $^{1}J(^{107/109}\text{Ag},^{31}\text{P})$ values) to be consistent with the remaining cases which possess protonated pendant groups (i.e. **1**, **2**, **3** and **4**).

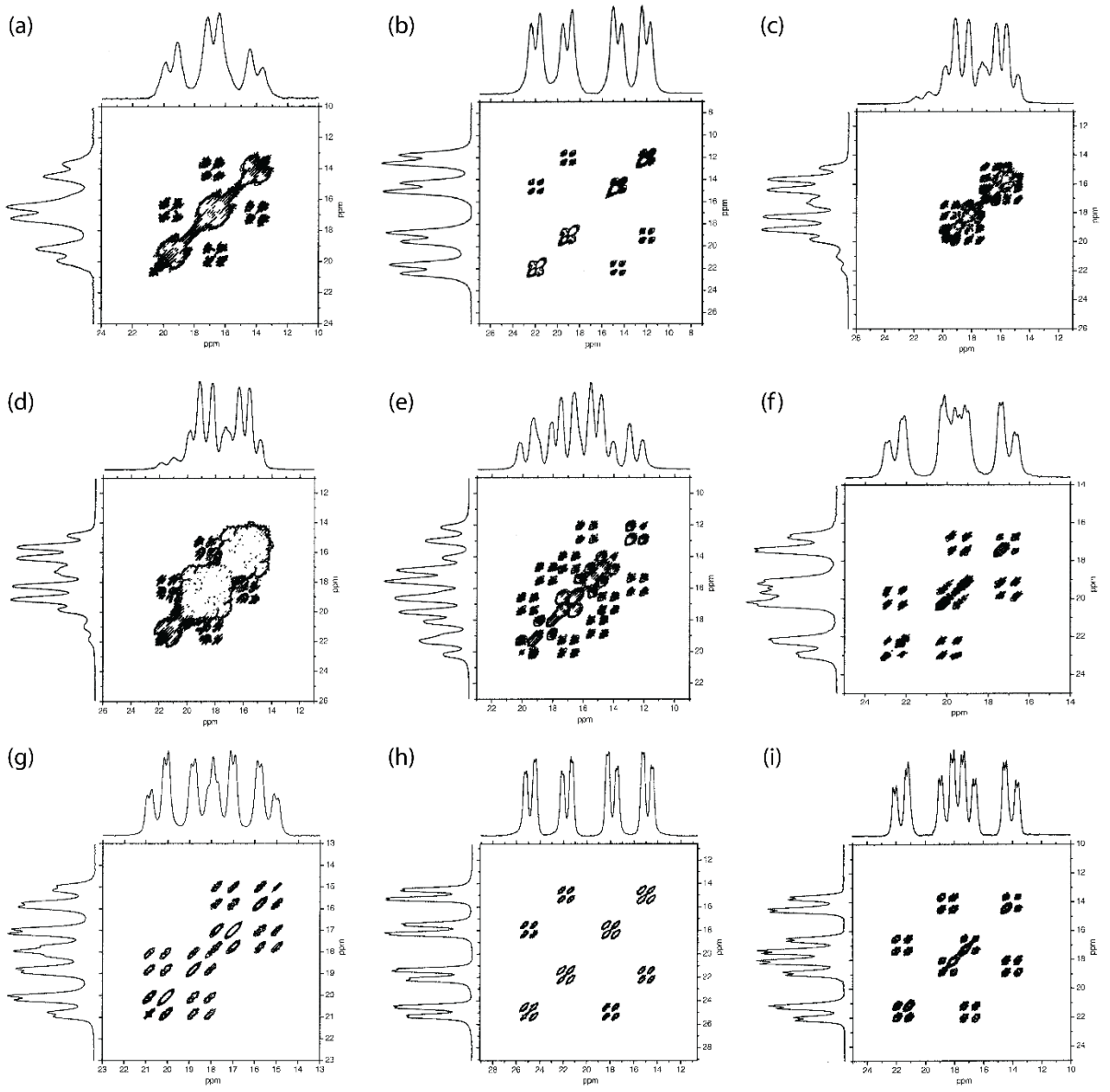

Figure 6. 1D ^{31}P CPMAS (F1 & F2 projections) and 2D ^{31}P-^{31}P CPCOSY MAS NMR data from (a) $[(Ph_3P)_2Ag(O_2CCH_2Ph)]$ **1**, (b) $[(Ph_3P)_2Ag(O_2CCHPh_2)]\cdot EtOH$ **2**, (c) $[(Ph_3P)_2Ag(O_2CC(CH_3)_3)]$ **3** with smaller vertical expansion, (d) $[(Ph_3P)_2Ag(O_2CC(CH_3)_3)]$ **3** with larger vertical expansion, (e) $[(Ph_3P)_2Ag(O_2CCH_2C(CH_3)_3)]$ **4**, (f) $[(Ph_3P)_2Ag(O_2CCF_3]$ **5β,** (g) $[(PPh_3)_2AgNO_3]$ **9*α***, (h) $[(PPh_3)_2AgNO_3]\cdot$toluene **11*α*** and (i) $[(PPh_3)_2AgNO_3]\cdot$toluene **11β**.

Table 5. ^{31}P NMR parameters measured from the 1D ^{31}P CPMAS and 2D ^{31}P-^{31}P CPCOSY MAS NMR data of complexes **1**, **2**, **3**, **4**, **5β**, **9α**, **11α** and **11β** reported in this work.

Compound	**δ(^{31}P)/ppm (±0.2 ppm)**	**^{1}J($^{107/109}$Ag,^{31}P)/Hz** [a] **(±3 Hz)**	**^{2}J(^{31}P,^{31}P)/Hz (±2 Hz)**
$[(Ph_3P)_2Ag(O_2CCH_2Ph)]$ **1**	5.9 8.5	443 439	125
$[(Ph_3P)_2Ag(O_2CCHPh_2)]\cdot EtOH$ **2**	3.8 11.0	414 470	125
$[(Ph_3P)_2Ag(O_2CC(CH_3)_3)]$ **3** (molecule 1, larger component from disorder)	7.1 8.5	426 455	124
$[(Ph_3P)_2Ag(O_2CC(CH_3)_3)]$ **3** (molecule 2, smaller component from disorder)	7.5 10.6	422 438	140
$[(Ph_3P)_2Ag(O2CCH_2C(CH_3)_3)]$ **4** (molecule 1)	6.3 8.8	426 455	125
$[(Ph_3P)_2Ag(O2CCH_2C(CH_3)_3)]$ **4** (molecule 2)	4.4 7.6	419 423	134
$[(Ph_3P)_2Ag(O_2CCF_3]$ **5β**	9.0 11.4	461 506	112
$[(PPh_3)_2AgNO_3]$ **9α**	7.5 9.3	489 492	127
$[(PPh_3)_2AgNO_3]\cdot$toluene **11α**	6.8 13.7	482 505	126
$[(PPh_3)_2AgNO_3]\cdot$toluene **11β**	6.0 10.5	471 510	136

[a] average value of ^{1}J(^{107}Ag,^{31}P) and ^{1}J(^{109}Ag,^{31}P) couplings.

The true effectiveness and utility of the 2D ^{31}P-^{31}P CPCOSY experiment is its ability to separate unresolved multiplets above and below the main diagonal in the COSY data representation which yields an unambiguous assignment of the two AB coupled sub-spectra. This feature becomes particularly valuable in complex arrangements where more than two Ag metal positions exist in the unit cell, or where positional disorder also leads to multiple $Ag(PPh_3)_2$ moieties. From Figures 6(a) and (b), compounds **1** and **2** are predisposed to a routine analysis of the ^{1}J(^{107,109}Ag,^{31}P) and ^{2}J(^{31}P,^{31}P) multiplet structure, but the corresponding 2D ^{31}P-^{31}P CPCOSY data for compound **3** present a very different scenario (see Figures 6 (c) and (d)). The

single crystal structure determination for **3** has identified positional disorder in the pendant t-butyl group which was modelled with constrained/well-defined geometries, and the 2D ^{31}P-^{31}P CPCOSY experiment is sensitive to these structural variations despite the large imbalance in the relative intensities of the species defined by this disorder. A comparison of Figures 6(c) and (d) shows that a significant vertical expansion of the baseline reveals the alternate structural form which exists at the 10 - 15% level. This phenomenon has been previously observed and quantified in the study of $[(Ph_3P)_2CuSCN]_n$ (thiocyanate) adducts using this technique.[64] Compound **4** represents a more complex and convoluted scenario where two chemically distinct Ag positions (i.e. four chemically distinct P positions) define the asymmetric unit cell; in this case the 2D ^{31}P-^{31}P CPCOSY data exhibited in Figure 6(e) clearly resolves all four $^{1}J(^{107,109}\text{Ag},^{31}\text{P})/^{2}J(^{31}\text{P},^{31}\text{P})$ multiplets. This example mirrors the 2D ^{31}P-^{31}P CPCOSY data from previously reported bis(triphenylphosphine) silver systems coordinated to $O_2C(OH)CHCH_2$ (lactate),[26] O_2CCH_3 (acetate and its monohydrate sesqiethanol solvate),[25,65] and $O_2CNC_5H_4$ (nicotinate)[66] shown in Figure S1, and summarized in Table S3 (Supplementary Material). In all of these cases, the 1D ^{31}P CPMAS spectra characterising the four chemically distinct P positions within each structure are complex and intractable, however, the 2D ^{31}P-^{31}P CPCOSY experiment transforms the representation to a more easily analysable 2D form which facilitates a deconvolution of the 1D data.

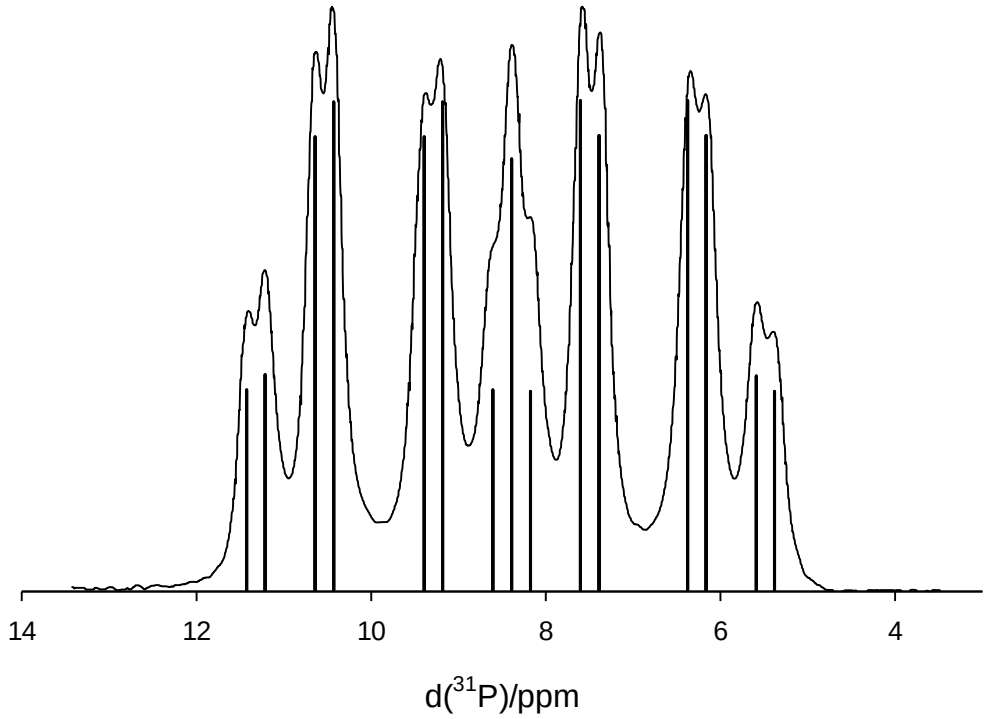

Figure 7. ^{31}P CPMAS NMR spectrum of $[(Ph_3P)_2Ag(NO_3)]\cdot$**9α** and stick diagram of the spectrum simulated as the AB part of an ABX system with δA = 7.47, δB = 9.33, J_{AX}^{107} = 455 Hz, J_{AX}^{109} =523 Hz, J_{BX}^{107} = 458 Hz, J_{BX}^{109} = 527 Hz, J_{AB} = 127 Hz.

The ^{31}P chemical shifts, and $^{1}J(^{107,109}Ag,^{31}P)$ and $^{2}J(^{31}P,^{31}P)$ coupling constants, summarized in Table 5 are consistent with the structures of the complexes reported in this work, and with previously reported carboxylate-based systems. It has previously been shown that one of the factors that determines the magnitude of $^{1}J(M,^{31}P)$ coupling constants in metal-phosphine complexes is the number of phosphine ligands coordinated to the metal atom M. An increase in the number of phosphine ligands results in a marked decrease in the magnitude of $^{1}J(M,^{31}P)$.[6,66,67,68] In the case of the formate complexes $[(Ph_3P)_nAg(O_2CH)]$, increasing the phosphine ligand coordination reduces $^{1}J(^{107,109}Ag,^{31}P)$ from ~430 (for n = 2) to ~230 Hz (for

n = 3).[6] The $^{1}J(^{107,109}Ag,^{31}P)$ value for the n = 2 case of the formate complexes is close to those values reported for the new carboxylate complexes in Table 5. Similarly, values such as $\delta(^{31}P)$ =7.6, 12.9; ^{1}J(AgP) 412, 501Hz; ^{2}J(PP) = 134 Hz obtained from the previously reported dihydrogen citrate complex $[(Ph_3P)_2Ag(H_2cit)]\cdot EtOH$ are central to ranges of values measured for the new carboxylate complexes summarized in Table 5.[9] It is interesting to note that various sized carboxylate-based anions of biological relevance (i.e. formate, acetate, citrate, lactate, nicotinate) can undergo bidentate coordination to the $Ag(Ph_3P)_2$ metal core,[6,9,25,26,65] and that the solid state 1D ^{31}P CPMAS and 2D ^{31}P-^{31}P CPCOSY experimental data are highly sensitive to their respective structural arrangements in each case.

As observed in Table 5, the $^{1}J(^{107,109}Ag,^{31}P)$ values measured from the nitrate complexes are generally larger than those for the carboxylate complexes. This observation is consistent with the greater strength of the Ag-P bonds reflected in the shorter Ag-P bond lengths for these complexes (see Table S1). In contrast, the values of $^{1}J(^{107,109}Ag,^{31}P)$ for the trifluoroacetate complex **5β** are higher than those for the other carboxylate complexes. This is due to the electron-withdrawing character of the trifluoromethyl group which reduces the base strength of the carboxyl group, thus resulting in weaker Ag-O bonds and stronger Ag-P bonds. This is thus reflected in the longer average Ag-O than in the shorter Ag-P bond lengths for this complex reported in Table S1. For compound **4** which contains two inequivalent $(Ph_3P)_2Ag$ centres in the complex molecules, the $^{1}J(^{107,109}Ag,^{31}P)$ values for molecule 1 are both greater than those for molecule 2 (see Table 5), thus correlating well with the fact that both Ag-P bond lengths in molecule 1 are shorter than those in molecule 2 (see Table S1). A plot of $^{1}J(^{107,109}Ag,^{31}P)$ *vs* the Ag-P bond length *d*(Ag,P) for the complexes in Table 5 (with assignment of the larger coupling constant to the shorter bond in each case) is shown in Figure 8. Also shown in this plot is the best fit curve for the corresponding data for $[Ag_2(PPh_3)_4(SeO_4)]\cdot 2H_2O$, which has four inequivalent P atoms with a range of Ag-P bond lengths and coupling constants similar to those

for the present nitrate and carboxylate complexes.[63] From this it is clear that the $^{1}J(^{107,109}\mathrm{Ag},^{31}\mathrm{P})$ *vs d*(AgP) dependence for these is closely similar to that for the selenate complex, which is also the case for the corresponding hydrogensulfate, hydrogenselenate and dihydrogenphosphate complexes.[63]

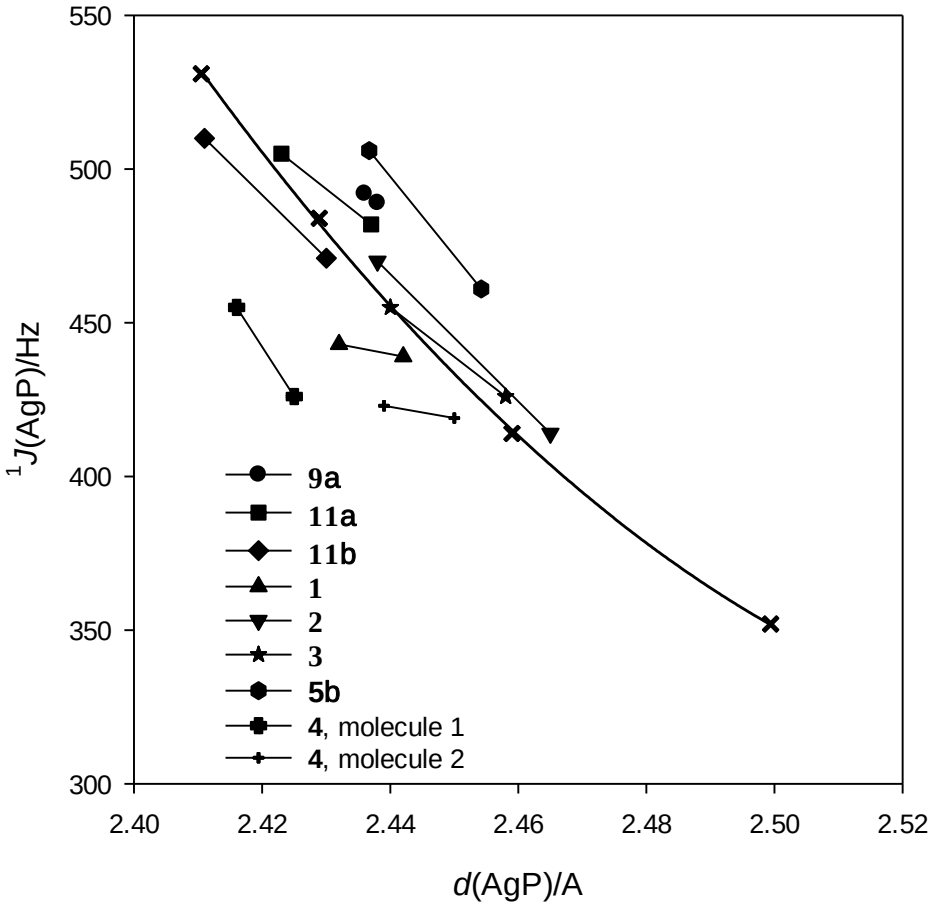

Figure 8. Plot of $^{1}J(^{107,109}\mathrm{Ag},^{31}\mathrm{P})$ vs. the Ag-P bond length *d*(AgP) for the nitrate and carboxylate complexes outlined in Table 5. The continuous curve is the best fit to the corresponding data for $[Ag_2(PPh_3)_4(SeO_4)]\bullet 2H_2O$ (symbols ×, reference 63).

Conclusions

Our study shows how the methods of solid-state NMR spectroscopy and single-crystal X-ray diffractometry complement each other in describing accurately and in detail, in this case, silver phosphine, carboxylate and nitrate interactions. Bond strength – bond length relationships can be established by both techniques. The new crystal structure elucidations in this work revealed, among other things, new polymorphs and isomorphs of known compounds. For such solid-state phenomena, analysis *via* the Hirshfeld Surface approach proved to be rewarding. Not only the intermolecular contacts and the outer molecular Hirshfeld Surfaces, but also the interplay between the coordination sphere of the central metal atom and the crystalline environment are informative with respect to the differences between polymorphs. This gives interesting insights into the different packing schemes that are decisive for the formation of different modifications of the same compound. Polymorphism seems to be not unusual in these systems, which is explained by shallow bending potentials around the silver atom facilitating different conformations of similar energy, which are stabilized by intermolecular interactions in the crystal packing. These energetic relationships were established by quantum-mechanical geometry optimizations and potential energy surface scans.

Acknowledgements

S.G. acknowledges the German Research Foundation (Deutsche Forschungsgemeinschaft, DFG) for funding within the Emmy Noether Project GR 4451/1-1. The National Computational Infrastructure (NCI) Facility is acknowledged for computing time under the project r65. J.V.H. acknowledges support for the solid state NMR instrumentation at Warwick used in this research which was funded by EPSRC and the University of Warwick, with additional partial funding being provided through the Birmingham Science City AM1 and AM2 projects which were supported by Advantage West Midlands (AWM) and the European Regional Development

Fund (ERDF). A.H.W. noted that he was grateful to Professor H.-B. Bürgi for helpful discussions.

The authors declare no conflicts of interest.

References

1. (a) R. J. Lancashire, in *Comprehensive Coordination Chemistry*, eds G. Wilkinson, R.D. Gillard, J. A. McCleverty, Pergamon, Oxford, **1987**, vol. 5, pp. 775ff; (b) M.C. Gimeno, A. Laguna, in *Comprehensive Coordination Chemistry II*, eds-in chief J.A. McCleverty, T.J. Meyer, Elsevier Pergamon **2004**, vol. 6, ed. D.E. Fenton, pp. 911ff.
2. C. E. Holloway, M. Melnik, W. A. Nevin, W. Liu, *J. Coord. Chem.* **1995**, *35*, 85.
3. A. Angel, A. V. Harcourt, *J. Chem. Soc.* **1902**, *81*, 1385.
4. A. Angel, *J. Chem. Soc.* **1906**, *89*, 345.
5. (a) G. A. Bowmaker, Effendy, J. V. Hanna, P. C. Healy, G. J. Millar, B. W. Skelton, A. H. White, *J. Phys. Chem.* **1995**, *99*, 3909; (b) an earlier determination is recorded in space group *Cc*: L.-S. Zheng, H.-H. Yang, Q.-E. Zhang, *Jiegou Huaxue (Chin. J. Struct. Chem.*) **1991**, *10*, 97 (CCDC: KIXCAV). (See also: (c) R. E. Marsh, *Acta Cryst. B* **1997**, *53*, 317 (KIXCAV01)).
6. G. A. Bowmaker, Effendy, J. V. Hanna, P. C. Healy, J. C. Reid, C. E. F. Rickard, A. H. White, *J. Chem. Soc., Dalton Trans.* **2000**, 753.
7. D. W. Hartley, G. Smith, D. S. Sagatys, C. H. L. Kennard, *J. Chem. Soc., Dalton Trans.* **1991**, 2735 (KOFZIO).
8. D. S. Sagatys, G. Smith, R. C. Bott, D. E. Lynch, C. H. L. Kennard, *Polyhedron* **1993**, *12*, 709 (LAPMEU).
9. G.A. Bowmaker, J.V. Hanna, B.W. Skelton, A.H. White, *Dalton Trans.* **2012**, *41*,

5409.

10. G. H. Penner, W. Li, *Inorg. Chem.* **2004**, *43*, 5588.

11. J. Shibata, K. Shimuzu, S. Satokawa, A. Satsuma, T. Hattori, *Phys. Chem. Chem. Phys.* **2003**, *5*, 2154.

12. K. Vehlow, K. Koehler, S. Blechert, S. Dechert, F. Meyer, *Eur. J. Inorg. Chem.* **2005**, 2727.

13. L. Jiang, Z. Wu, D. Wu, W. Yang, R. Jin, *Nanotechnology* **2007**, *18* 185603.

14 Z. S. Pillai, P. V. Kamat, *J. Phys. Chem. B* **2004**, *108*, 945.

15. O. Silman, L. A. Bumm, R. Callaghan, C. G. Blatchford, M. Kerker, *J. Phys. Chem.* **1983**, *87*, 1014.

16. J. Clarkson, C. Campbell, B. N. Rospendowski, W. E. Smith, *J. Raman. Spectroscopy* **1991**, *22*, 771.

17. C. H. Munro, W. E. Smith, M. Garner, J. Clarkson, P. C. White, *Langmuir* **1995**, *11*, 3712.

18. C. Rodger, W. E. Smith, G. Dent, M. Edmondson, *J. Chem. Soc., Dalton Trans.* **1996**, 791.

19. K. K. Caswell, C. M. Bender, C. J. Murphy, *Nano Letters* **2003**, *3*, 667.

20. F.-K. Liu, P.-W. Huang, Y.-C. Chang, F.-H. Ko, T.-C. Chu, *J. Mater. Res.* **2004**, *19*, 469.

21. S. Eckhardt, P. S. Brunetto, J. Gagnon, M. Priebe, B. Giese, K. M. Fromm, *Chem. Rev.* **2013**, *113*, 4708.

22. V. Sambhy, M. M. MacBride, B. R. Peterson, A. Sen, *J. Am. Chem. Soc.* **2006**, *128*, 9798.

23. G. A. Bowmaker, Effendy, J. V. Hanna, P. C. Healy, S. P. King, C. Pettinari, B. W. Skelton, A. H. White, *Dalton Trans.* **2011**, *40***,** 7210.

24. (a) S.-W. Ng, A. H. Othman, *Acta Cryst C* **1997**, *53*, 1396, describing $[(Ph_3P)_2Ag(O_2CCH_3)]$ as both unsolvated (ACPSAG01) and sesquihydrate ($1.5H_2O$) (ROGTIQ) phases. See also (b) B. Femi-Onadenko, *Z. Kristallogr.* **1980**, *152*, 1159 (ACPSAG).

25. J. V. Hanna, S.-W. Ng, *Acta Cryst. C* **1999**, *55*, 9900031, describing the ethanol monosolvate monohydrate (HIPVIL), a redetermination/correction of the sequihydrate.

26. J. V. Hanna, S.-W. Ng, *Acta Cryst. C* **2000**, *56*, 24 (GUGVAF).

27. S.-W. Ng, *Acta Cryst. C* **1998**, *54*, 743 (NOZPIB).

28. D.A. Edwards, R. M. Harker, M. F. Mahon, K. C. Molloy, *Inorg. Chim. Acta* **2000**, *328*, 134.

29. D. J. Darensbourg, M. W. Holtcamp, B. Khandelwal, J. H. Reibenspies, *Inorg. Chem.* **1995**, *34*, 5390 (ZIMMUD, ZIMNAK).

30. N. Marsich, A. Camus, G. Nardin, *J. Organomet. Chem.* **1982**, *239*, 429 (BOMFUE).

31. (a) M. G. B. Drew, A. H. bin Othman, D. A. Edwards, R. Richards, *Acta Cryst. B* **1975**, *31*, 2695 (ACPHCU); (b) A. S Batsanov, Y. T. Struchkov, *Koord. Khim.* **1982**, *8*, 1141 (ACPHCU01); (c) D. J. Darensbourg, M. W. Holtcamp, E. M. Longridge, K. K. Klausmeyer, J. H. Reibenspies, *Inorg. Chim. Acta* **1994**, *227*, 223 (ACPHCU02).

32. R. D. Hart, P. C. Healy, G. A. Hope, D. W. Turner, A. H. White, *J. Chem. Soc., Dalton Trans.* **1994**, *773* (WEPKAD, WEPKEH, WEPJUW, WEPJIK, WEPJEG).

33. (a) G. G. Messmer, G. J. Palenik, *Inorg. Chem.* **1969**, *8*, 2750 (NITPPC20); (b) R. D. Hart, P. C. Healy, M. L. Peake, A. H. White, *Aust. J. Chem.* **1998**, *51*, 67 (NITPPC01); (c) R.-N. Yang, T.-X. Li, Y.-A. Sun, X.-Y. Hu, D.-M. Jin, B.-S. Luo, *Jiegou Huaxue* (*Chin. J. Struct. Chem.*) **2000**, *19*, 126, (NITPPC02); (d) a useful addition is provided by the structure of $[\{(p\text{-tol})_3Ag(O_2NO)]$: C. Pettinari, G.G. Lobbia, G. Sclavi, D. Leonesi, M. Colapietro, G. Portalone, *Polyhedron* **1995**, *14*, 1709 (ZACZUY).

34. P. Römbke, A. Schier, H. Schmidbaur, S. Cronje, H. Raubenheimer, *Inorg. Chim. Acta,* **2004**, *357,* 235.

35. (a) P. F. Barron, J. C. Dyason, P. C. Healy, L. M. Engelhardt, B. W. Skelton, A. H. White, *J. Chem. Soc., Dalton Trans.* **1986**, 1965 (DUSZOG); redeterminations are described in (b) Z. Lansun, Y. Wenbin, Y. Huahui, *Xiamen Dax. Xuebao (Chin.); J. Xiamen Univ. (Nat. Sci.)* **1998**, *27,* 437 (DUSZOG01); (c) F. Cheng, W. Levason, M. Webster, CSD, Private communication (**2009**) (DUSZOG02).

36. C. S. W. Harker, R. T. Tiekink, *Acta Cryst. C* **1989**, *45,* 1815 (SAYZAT).

37. P. G. Jones, *Acta Cryst. C*, **1993**, *49,* 1148 (WANFAS).

38. G. M. Sheldrick, *Acta Crys. C* **2015**, *71,* 3.

39. A. Pines, M. G. Gibby, J. S. Waugh, *J. Chem. Phys.* **1973**, *59*, 569.

40. E. R. Andrew, A. Bradbury, R. Eades, *Nature* **1958**, *182*, 1659.

41. E. O. Stejskal, J. Schaefer, *J. Magn. Reson.* **1975**, *18*, 560.

42. G. Bodenhausen, R. L. Vold, R. R. Vold, *J. Magn. Reson.* **1980**, *37*, 93.

43. D. Marion, K. Wuthrich, *Biochem. Biophys. Res. Commun.* **1983**, *113*, 967.

44. T. Allman, *J. Magn. Reson.* **1989**, *83*, 637.

45. a) J. V. Hanna, M. E. Smith, S. N. Stuart, P. C. Healy, *J. Phys. Chem.* **1992**, *96,* 7560. b) J. V. Hanna, R. D. Hart, P. C. Healy, B. W. Skelton, A. H. White, *J. Chem. Soc., Dalton Trans.* **1998**, 2321.

46. Y. Zhao, D. G. Truhlar, *J. Phys. Chem*. *A* **2005**, *109*, 5656.

47. F. Neese, *WIREs Comput. Mol. Sci.* **2012**, *2*, 73.

48. L. Goerigk, S. Grimme, *Phys. Chem. Chem. Phys.* **2011**, *13*, 6670.

49. T. H. Dunning Jr., *J. Chem. Phys*. **1989**, *90*, 1007.

50. D. E. Woon, T. H. Dunning Jr., *J. Chem. Phys*. **1993**, *98*, 1358.

51. K. A. Peterson, C. Puzzarini, *Theor. Chem. Acc*. **2005**, *114*, 283.

52. (a) M. A. Spackman, D. Jayatilaka, *Cryst. Eng. Comm.* **2009**, *11*, 19.

(b) A. J. Edwards, C. F. Mackenzie, P. R. Spackman, D. Jayatilaka, M. A. Spackman, *Faraday Discuss.* **2017**, *203*, 93.

(c) S. K. Wolff, D. J. Grimwood, J. J. McKinnon, M. J. Turner, D. Jayatilaka, M. A. Spackman, Crystal Explorer (Version 3.0), University of Western Australia, **2010**.

53. M. A. Spackman, J. J. McKinnon, *Cryst. Eng. Comm*. **2002**, *4*, 378.

54. J. J. McKinnon, M. A. Spackman, A. S. Mitchell, *Acta Cryst. B* **2004**, *60*, 627.

55. J. J. McKinnon, D. Jayatilaka, M. A. Spackman, *Chem. Commun*. **2007**, 3814.

56. M. A. Spackman, J. J. McKinnon, D. Jayatilaka, *Cryst. Eng. Comm.* **2008**, *10*, 377.

57. J. Bernstein, *Cryst. Growth Des.* **2011**, *11*, 632.

58. (a) J. V. Hanna, S. W. Ng, *Acta Cryst. C* **1999**, *55*, 9900029 (HIPVEH); (b) A. Cingolani, Effendy, M. Pellei, C. Pettinari, C. Santini, B. W. Skelton, A. H. White, *Inorg. Chem*. **2002**, *41*, 6633 (HIPVEH01).

59. J. A. Halfen, W. B. Tolman, *Acta Cryst. C* **1995**, *51*, 215 (HIBPUD).

60. L. Nørskov-Lauritsen, H.-B. Bürgi, *J. Comp. Chem.* **1985**, *6*, 216.

61. O. Wu, R. Wasylishen, *Organometallics* **1992**, *11*, 3242.

62. R. K. Harris, *Nuclear Magnetic Resonance Spectroscopy*, Longman, London, **1986**, pp. 54–57.

63. G. A. Bowmaker, J. V. Hanna, C. E. F. Rickard, A. S. Lipton, *J. Chem. Soc., Dalton Trans.* **2001**, 20.

64. G. A. Bowmaker, J. V. Hanna, R. D. Hart, P. C. Healy, S. P. King, F. Marchetti, C. Pettinari, B. W. Skelton, A. Tabacaru, A. H. White. *J. Chem. Soc., Dalton Trans* **2012**, *41*, 7513.

65. S. W. Ng, A. H. Othman, Acta Cryst. C **1997**, *53*, 1396.

66. L. J. Baker, G. A. Bowmaker, D. Camp, Effendy, P. C. Healy, H. Schmidbaur, O.

Steigelmann, A. H. White, *Inorg. Chem.* **1992**, *31*, 3656.

67. E. C. Alyea, J. Malito, J. H. Nelson, *Inorg. Chem.* **1987**, *26*, 4294.

68. E. L. Muetterties, C. W. Alegranti, *J. Am. Chem. Soc.* **1972**, *94*, 6386.